

Tracking Objects with 3D Representation from Videos

Jiawei He¹ Lue Fan¹ Yuqi Wang¹ Yuntao Chen²
Zehao Huang³ Naiyan Wang³ Zhaoxiang Zhang^{1,2}
¹ CASIA ² CAIR, HKISI.CAS ³ TuSimple

{hejiawei2019, fanlue2019, wangyuqi2020, zhaoxiang.zhang}@ia.ac.cn

{chenyuntao08, zehaohuang18, winsty}@gmail.com

Abstract

Data association is a knotty problem for 2D Multiple Object Tracking due to the object occlusion. However, in 3D space, data association is not so hard. Only with a 3D Kalman Filter, the online object tracker can associate the detections from LiDAR. In this paper, we rethink the data association in 2D MOT and utilize the 3D object representation to separate each object in the feature space. Unlike the existing depth-based MOT methods, the 3D object representation can be jointly learned with the object association module. Besides, the object’s 3D representation is learned from the video and supervised by the 2D tracking labels without additional manual annotations from LiDAR or pretrained depth estimator. With 3D object representation learning from Pseudo 3D object labels in monocular videos, we propose a new 2D MOT paradigm, called P3DTrack. Extensive experiments show the effectiveness of our method. We achieve new state-of-the-art performance on the large-scale Waymo Open Dataset.

1. Introduction

Multiple Object Tracking (MOT) is the core component of the perception system for many applications, such as autonomous driving and video surveillance. In the deep learning era, metric learning helps the network to learn better object affinity between frames for object association in MOT [56, 3, 16]. Another hot trend is jointly learning object detection and association, termed as end-to-end MOT [32, 59, 68]. In these methods, they use the shared query to generate the object’s bounding box in each frame belonging to the same track. This kind of design makes the neural network jointly learn object representation and data association across frames. Previous attempts demonstrate that precise association is crucial in MOT. However, in 2D MOT, object association remains a significant challenge due to object occlusion. The presence of many partially visible objects in congested scenarios like shopping malls and traf-

fic jams makes incorrect association nearly impossible to prevent. Several approaches have aided the data association module with complex appearance models and image-space motion models to address the challenging 2D data association. Despite the efficacy of these techniques, they do not target the main problem of object association, that is, trying to associate 3D objects in 2D image space.

Conversely, in 3D MOT, many works demonstrate that object association is nearly a trivial problem, even with a simple motion model. ImmortalTracker [51], in particular, reveals that using the 3D Kalman Filter to model motion from the LiDAR 3D bounding boxes, the wrong association only occurs *once* in the entire Waymo Open Dataset (WOD) dataset. This significant gap between 2D and 3D MOT reveals that association in a higher dimension space is much simpler than in a low-dimensional space. Therefore, inspired by this observation, this paper aims to address the 2D object association problem in a 3D space.

Recent works [23, 7] explore the most straightforward way to lift 2D association to 3D space, that is utilizing the off-the-shelf depth model. However, such methods are not effective enough for three reasons. (1) It is hard to estimate the scene-level depth from the monocular image. (2) The camera’s intrinsic parameters are different, so the pretrained depth estimation model has limited generalization ability in the tracking scenes. (3) Association with explicit depth is sub-optimal since the depth estimation and the association part are isolated without joint optimization. Meanwhile, without joint optimization, the association is also sensitive to the noise of explicit depth.

Distinct from these works, we want to learn the representation containing 3D position information for the objects, and the representation can be jointly learned with the association module, as shown in Fig. 1. Besides, due to the expensive cost and the additional sensors (e.g., LiDAR) to obtain the 3D annotations, we want to dig the 3D object representation only from 2D tracklet labels annotated in the videos. In this paper, we propose a new video-based 3D representation learning framework and the 2D Multiple

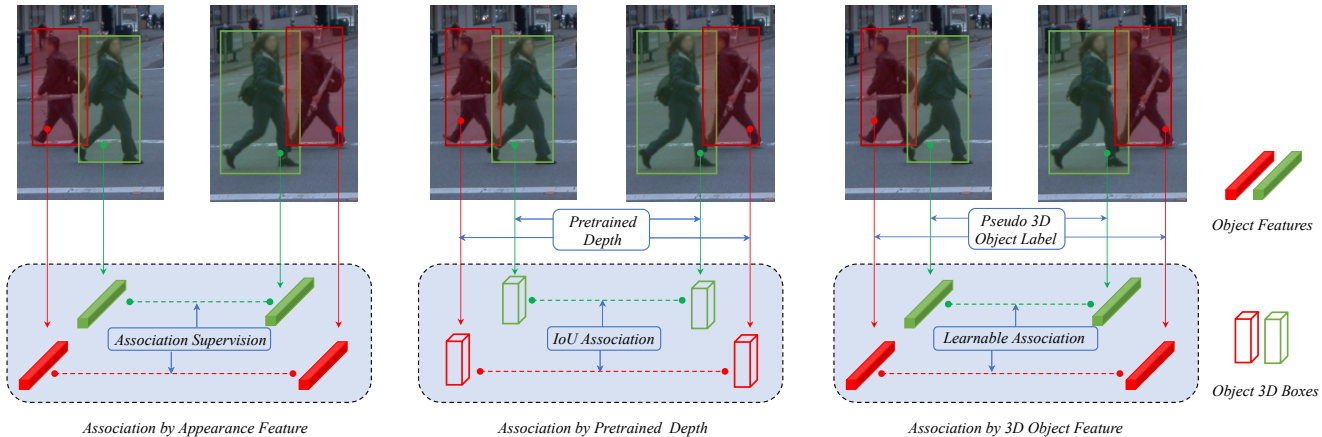


Figure 1: **Three streams in the field of 2D MOT.** Left: Association by appearance feature learning. Middle: Association by lifted 3D objects from the pretrained depth model. Right: Association by learnable 3D representation from pseudo 3D object labels.

Object Tracking algorithm with the 3D object representation, called P3DTrack. P3DTrack mainly consists of three parts: (1) pseudo 3D object label generation, (2) jointly learning framework including 3D object representation and object association learning, (3) a simple yet effective on-line tracker with learned 3D object representation. As for pseudo 3D object label generation, inspired by Structure-from-Motion [44], the scene can be reconstructed in 3D space from the camera motion. The 3D object is located as a part of the reconstructed scene. Fortunately, with the 2D bounding boxes in video frames, we can find the 3D object’s reconstructed point clouds lie in the intersection area of the object frustums of multiple frames. By finding the main cluster of the reconstructed object point clouds, the 3D object position can be annotated as the center of the cluster. After that, the pseudo label offers P3DTrack supervision to learn the 3D representation of objects. The representations are then fed into a graph-matching-based object association module for joint optimization. Then the tracker can track the objects frame-by-frame with the robustness of heavy occlusion and similar appearance. In summary, our work has the following contributions:

- We propose a new online 2D MOT paradigm, called P3DTrack. P3DTrack utilizes the jointly learned 3D object representation and object association.
- We design the 3D object representation learning module, called 3DRL. With 3DRL, the object’s 3D representation is learned from the video and supervised by the 2D tracking labels without any additional annotations from LiDAR or pretrained depth estimator.
- The extensive experiments on the large-scale Waymo

Open Dataset show that we achieve new state-of-the-art performance.

2. Related Work

2.1. Multiple Object Tracking

Multiple Object Tracking (MOT) aims to associate the same object in a video. To track the object, linear motion models, like Kalman Filter (KF) [21], and appearance models [56] from re-identification are the core components in the tracker. However, the 2D MOT task suffers from object occlusion, camera shake, and similar appearance. Many methods tend to use graph neural networks [3, 16] and attention mechanism [59, 32, 68] to aggregate the object features across intra- and inter-frames. Some researchers reveal that learning object features and object association jointly [57, 16] can help to obtain more discriminative object features. Transformer-based end-to-end MOT [59, 32] build a new paradigm with track query to represent a whole track. Score-based detection selection, such as ArTIST [41] and ByteTrack [62], also helps the tracker to keep high-quality detections and tracks. In 3D MOT, 3D Kalman Filter is a very common practice. AB3DMOT [55] propose a simple KF-based online tracker. Recent work [51] has revealed that with only 3D KF, LiDAR-based 3D MOT is almost association error-free evaluated on the mainstream autonomous driving datasets.

Recently, with the development of monocular 3D object detection [36, 61, 53] and multi-camera 3D object detection [54, 20, 26], camera-based 3D multiple object tracking is emerging. In the early years, Mono3DT [18] is the first to learn monocular 3D object detection and 3D multiple object tracking. MUTR3D [60] extends the transformer-

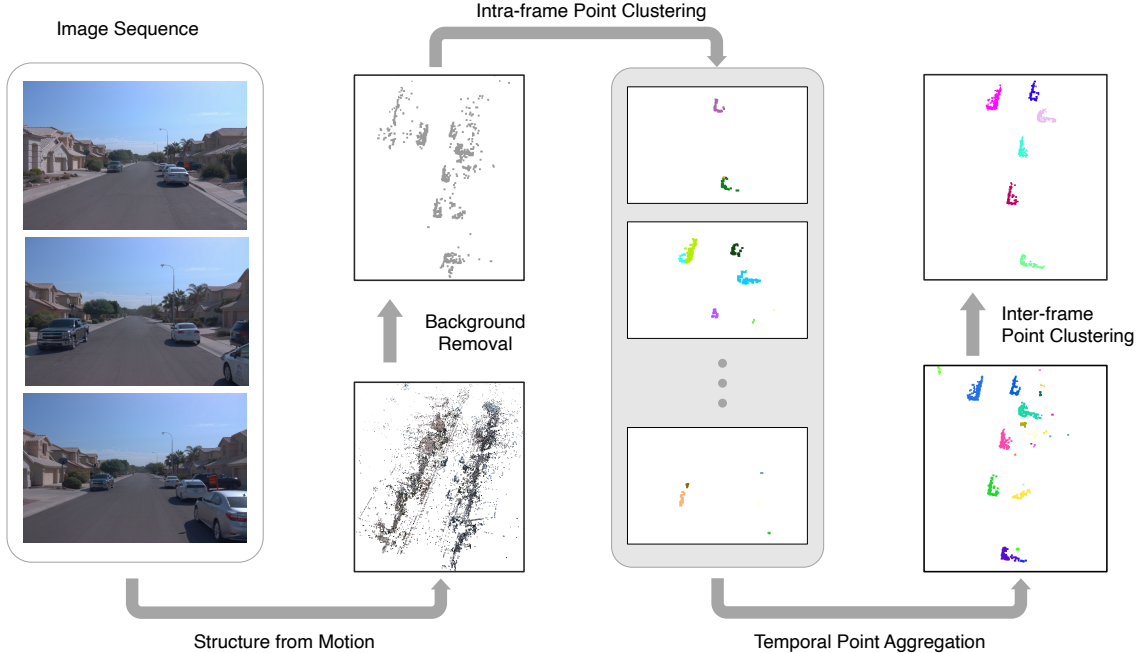


Figure 2: **Illustration of pseudo 3D object label generation process.** After reconstructing the scene with Structure-from-Motion, intra-frame and inter-frame point clustering are adopted. The pseudo 3D object label can be defined as the barycenter of the cluster.

based tracker to camera-based 3D MOT. PF-Track [35] is the new state-of-the-art camera-based 3D MOT method utilizing past and future trajectory reasoning. Although these methods are a little similar to ours on the 3D representation learning level, we focus on different key problems. We care more about whether the hidden 3D information in the video can help the association in 2D MOT, so we do not use the manually annotated 3D object labels.

2.2. 3D Representation from Video

In this subsection, we visit the existing work representing objects in the 3D space, especially for learning from videos. Generally speaking, recovering the 3D representation from a video can be divided into scene reconstruction and representing objects in 3D space. With the help of multi-view geometry, Structure from Motion (SfM) [44] is a practical algorithm to estimate the depth of each keypoint and recover the sparse 3D structure of the static scene from a movable camera. Multi-view Stereo (MVS) [45] is the dense scene reconstruction method from every pixel. In robotics, Simultaneous Localization and Mapping (SLAM) [6, 34, 33] utilizes a continuous video clip to estimate the robot’s ego-pose and construct a sparse or dense map for planning and controlling.

In the perception field, a common practice is representing 3D objects with cuboid bounding boxes, defined as the

3D object detection task [46, 11]. However, most vision-based 3D object detection methods [36, 61] leverage the neural network to fit the cuboid labels from *LiDAR* annotations. As for 3D video object detection, inspired by scene reconstruction, DfM [52] and BEVStereo [25] refine the object depth from the video. BA-Det [15] is the first to represent the consistent 3D object explicitly in the video via object-centric bundle adjustment.

Another kind of 3D representation from the video is to learn video consistent depth. SfMLearner [65] is a pioneer work taking view synthesis as supervision. [31, 64] are the methods of learning consistent video depth and smooth scene flow with test-time training. These methods learn from traditional Structure-from-Motion and treat temporal warping consistency as geometric constraints. However, our method learns object 3D representation rather than the dense scene-level depth.

3. Preliminary: Structure-from-Motion

Given a series of images $\{\mathbf{I}^t\}$, Structure-from-Motion is to reconstruct the 3D scene with 3D points $\{\mathbf{P}_i\}$ and estimate camera motion $\{\mathbf{T}^t\}$ in the global frame. In the SfM system, local features $\{\mathbf{f}_i^t\}$ are extracted at the location of keypoints $\{\mathbf{p}_i^t\}$ in each frame firstly using traditional feature extractor SIFT [28], or deep learning-based feature ex-

tractor D2-Net [9] and SuperPoint [8]. Then the extracted local features are matched as pairs $\{(\mathbf{p}_i^t, \mathbf{p}_i^{t'})\}$ between different frames and the keypoint tracklets $\{(\mathbf{p}_i^1, \dots, \mathbf{p}_i^T)\}$ are generated. With triangulation, the initial 3D location of matched keypoint pairs can be obtained. And utilizing bundle adjustment in multi-frames, the camera poses $\{\mathbf{T}^{t*}\}$ in each frame and the global locations $\{\mathbf{P}_i^*\}$ of each keypoint are optimized by minimizing the reprojection errors of the extracted keypoints. In practice, COLMAP [44] is a fast and widely-used SfM framework.

4. Methodology

In this section, we introduce the new 2D MOT paradigm with 3D object representation. The pipeline contains three parts: (1) a CenterNet [67]-based 2D object detection branch; (2) a joint learning framework to learn 3D object representation and object association; (3) an online 2D tracker with 3D object representation in the inference stage, called P3DTrack.

The 2D object detection branch is mainly from CenterNet [67], with DLA-34 [58] backbone fusing multi-scale features. The output feature map of the backbone is with stride 4. The detection heads include the center heatmap prediction head and the bounding box regression head. Following FCOS [47], the regression target is (l^*, t^*, r^*, b^*) , corresponding to the distance from the regression center to the sides of the bounding box. In the inference stage, non-maximum suppression (NMS) is performed as a post-process, different from the original CenterNet.

4.1. Generating Pseudo 3D Object Labels

The existing works, which either utilize the pretrained depth estimator supervised by LiDAR or learn the object representation with human-annotated 3D labels, are not pure 2D MOT paradigms. We want to learn the 3D object representation only from the monocular video. In this section, as shown in Alg. 1 and Fig. 2, we introduce how to generate the pseudo 3D object labels from the video clips taken from the surrounding cameras based on the Structure-from-Motion technique.

Given a video clip $\mathcal{V} = \{\mathbf{I}_t^k | t = 1, 2, \dots, T\}$ taken from the surrounding cameras $\{c_k\}$, we first extract the 2D keypoints $\mathbf{p}_{t,k}^i = [u_i, v_i]^\top$, ($i = 1, 2, \dots, n$) and the corresponding local features $\mathcal{F}_t = \{\mathbf{f}_{t,k}^i\}$ utilizing SuperPoint [8] network. The local feature matching network is from SuperGlue [43], a GNN-style network aggregating spatial and temporal information to make local features discriminative. Suppose that intrinsic of each camera \mathbf{K}_{c_k} and the camera pose $\mathbf{T}_t^k = [\mathbf{R}_t^k | \mathbf{t}_t^k]$ at time t are given, then SfM system can be applied to obtain the 3D position of each keypoint \mathbf{P}_i in the global frame by solving the nonlinear least square

Algorithm 1: Generating pseudo 3D object labels from a video.

Input: video clip \mathcal{V} , camera intrinsic $\{\mathbf{K}_{c_k}\}$, camera pose $\{\mathbf{T}_t^k\}$, 2D bounding box with id $\{\mathbf{B}_j^t\}_{j=1}^{n_d}$
Output: pseudo 3D object label $\{\mathbf{o}_j^{t*}\}$

- 1 $\{\mathbf{P}_i^*\}_{i=1}^n \leftarrow \text{SfM}(\mathcal{V}, \{\mathbf{K}_{c_k}\}, \{\mathbf{T}_t^k\})$
- 2 $\mathcal{P} \leftarrow \emptyset$
- 3 // IntraPC for each object
- 4 **for** $j \in [1, n_d]$ **do**
- 5 **for** $t \in [1, T]$ **do**
- 6 $\mathcal{P}_j^t \leftarrow \text{IntraPC}(\{\mathbf{P}_i^*\}, \mathbf{B}_j^t)$
- 7 $\mathcal{P} \leftarrow \mathcal{P} \cup \mathcal{P}_j^t$
- 8 // InterPC for all foreground points \mathcal{P} to generate n'_d clusters
- 9 $\{\mathcal{P}_{j'}^{n'_d}\}_{j'=1}^{n'_d} \leftarrow \text{InterPC}(\mathcal{P})$
- 10 // Assign ID to the point clusters
- 11 $\{\mathcal{P}_j^*\}_{j=1}^{n_d} \leftarrow \text{MatchID}(\{\mathcal{P}_{j'}^{n'_d}\}, \{\mathbf{B}_j^t\})$
- 12 // Find barycenter for each cluster and transform to each camera frame
- 13 $\{\mathbf{o}_j^{t*}\} \leftarrow \text{FindCenter\&Transform}(\{\mathcal{P}_j^*\}, \{\mathbf{T}_t^k\})$
- 14 **return** $\{\mathbf{o}_j^{t*}\}$

problem

$$\{\mathbf{P}_i^*\}_{i=1}^n = \arg \min_{\{\mathbf{P}_i\}_{i=1}^n} \frac{1}{2} \sum_{i=1}^n \sum_{t=1}^T \|\mathbf{p}_i^t - \Pi(\mathbf{T}_t^k, \mathbf{P}_i, \mathbf{K}_{c_k})\|^2. \quad (1)$$

where $\Pi(\cdot)$ is the reprojection function from the world frame to the image frame with the camera pose and the intrinsic parameters. Note that not all scenes can be reconstructed well. When the camera movement is relatively small, the reconstruction performance is bad. So, we filter the videos with a low speed of ego-motion. Besides, in the traditional SfM system, the static scene can be well-reconstructed but the moving objects can not be reconstructed because their movement is not the same as the ego-motion and are filtered in the outlier filtering step by RANSAC [13]. Thanks to the generalization capability of the deep neural network, these inherent problems of traditional SfM are easily solved. Please refer to Sec. 4.2 for more details.

After reconstructing the 3D points in the global frame, we filter the points that can be projected to the foreground regions in the images, and then we perform the Intra-frame Point Clustering (Intra-PC) to select the main connected component of the 3D keypoints for each object \mathbf{B}_j^t :

$$\mathcal{P}_j^t = \{\mathbf{P}_i\}_{i=1}^m = \text{IntraPC}(\{\mathbf{P}_i^* | \Pi(\mathbf{T}_t^k, \mathbf{P}_i^*, \mathbf{K}_{c_k}) \in \mathbf{b}_j^t\}), \quad (2)$$

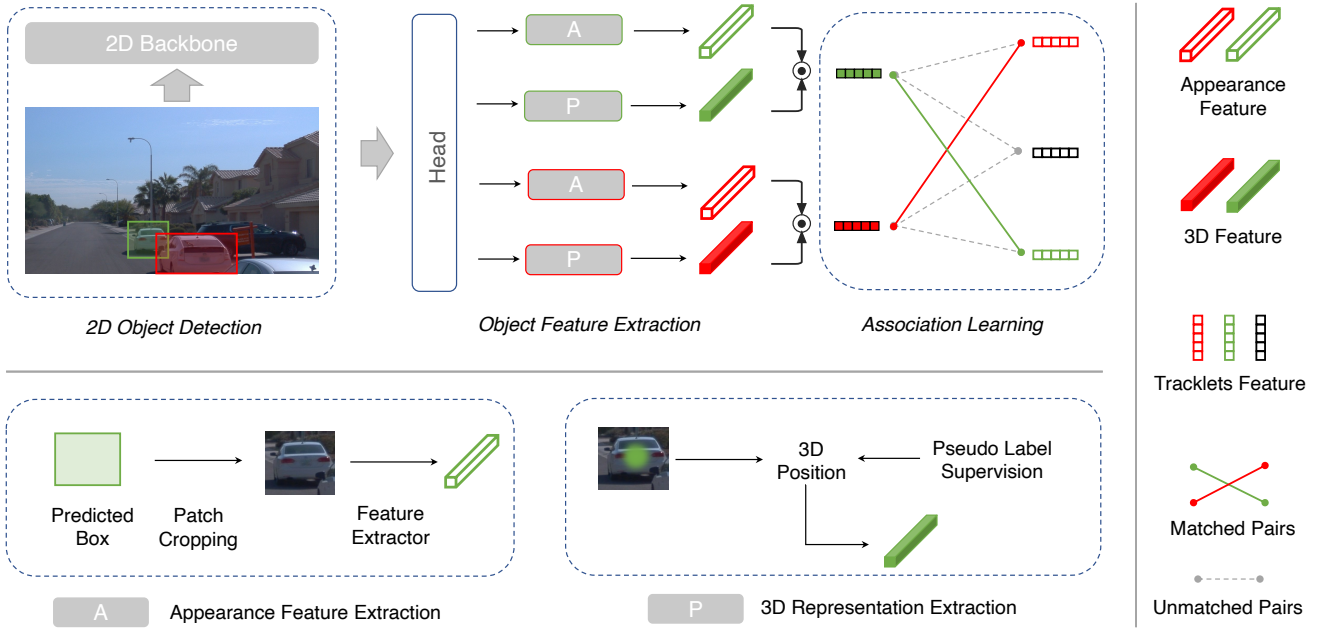


Figure 3: **Pipeline of P3DTrack.** The object detector is based on CenterNet. We learn the 3D object representation and data association module jointly from the pseudo 3D object labels.

where \mathbf{b}_j^t is the region within the ground truth 2D bounding box \mathbf{B}_j^t . The index $j \in [1, n_d]$ means the identity of the object. The distance threshold of a cluster is δ . That means we only consider the biggest cluster belonging to the object, which can filter the noise points in the background regions or caused by keypoint mismatching.

Besides, we cluster the 3D keypoints for the second stage, called Inter-frame Point Clustering (Inter-PC), to further filter the noise points in the global frame for all objects together:

$$\{\mathcal{P}_{j'}\}_{j'=1}^{n'_d} = \text{InterPC}\left(\bigcup_{t,j} \mathcal{P}_j^t\right). \quad (3)$$

We finally generate n'_d object clusters. In each cluster, the number of points must exceed the threshold κ . In general, the cluster number is less than the number of tracks, so some tracks will not be assigned to the 3D object labels. In 3D object representation learning, these objects are only supervised by 2D representation labels and be ignored in 3D.

After clustering the 3D points, we should match the cluster with the maximum probability corresponding to the tracklet. We define the matching strategy that if the cluster can be only projected into *one* bounding box \mathbf{B}_j with id j , we match the cluster to the tracklet j . If not, we assign the cluster to the tracklet whose 2D bounding box can involve the maximum number of the reprojected points. Note that we only label static objects and this matching strategy guarantees the same 3D object position in the global frame for a tracklet, so the 3D object representation learning can keep

consistent in a tracklet and the association can be learned well.

To supervise the 2D bounding box with 3D representation, we need to define the target 3D location for each ground truth 2D bounding box. Two kinds of definitions are common in practice. The first is the barycenter, which is the average 3D position of the cluster in the global frame. The second definition is the minimum circumscribed cuboid for the cluster. In the experiments, we find that with these two definitions, tracking performance is nearly the same. So, we finally choose the barycenter $\mathbf{o}_j^{t*} = [x_j^{t*}, y_j^{t*}, z_j^{t*}]^T$ in the camera frame as the 3D position target for the object. In summary, we obtain the initial 3D representation with a cluster of 3D points for each tracklet. Then we need to learn the generalized 3D representation for each object and utilize the 3D object representation to associate the objects between frames.

4.2. 3D Representation and Association Learning

3D object representation learning. In this subsection, we introduce the proposed 3D object representation learning module, called the 3DRL, shown in Fig. 3. 3DRL module is an additional head of the object detection model CenterNet to represent 3D attributes of the objects, with a shared DLA-34 backbone. We denote the output of the backbone feature as $\mathbf{F}_t \in \mathbb{R}^{H \times W \times C}$. Like FairMOT [63], we choose the 2D object center position to extract the 3D feature ${}^{(3D)}\mathbf{f}_j^t$ of the object \mathbf{B}_j^t , which will be further utilized for object tracking. In the following, we will explain how to extract the 3D ob-

ject feature. The 3D branch first uses MLPs as the feature encoder to encode the backbone features, and the 3D object feature is

$$\mathbf{o}_j^t = \text{MLP}(\mathbf{F}_t)[c_j(u), c_j(v)], \quad (4)$$

where $[c_j(u), c_j(v)]$ is the position of 2D object center on the feature map \mathbf{F}_t , and $\mathbf{o}_j^t = [x_j^t, y_j^t, z_j^t]^\top$ is the 3D position of the object center in the camera frame. Learned from the generated pseudo 3D object labels, we define the 3D object position auxiliary loss with uncertainty following [22, 61],

$$\mathcal{L}_{3D} = \frac{\|\mathbf{o}_j^t - \mathbf{o}_j^{t*}\|_1}{\sigma^2} + \log(\sigma^2), \quad (5)$$

where σ^2 is the learnable 3D position uncertainty for the object j .

Then the 3D object representation is predicted by an additional fully-connected layer

$${}^{(3D)}\mathbf{f}_j^t = \mathbf{f}c(\mathbf{o}_j^t). \quad (6)$$

Note that even though only the position of the static object is supervised, the network can easily make the 3D position prediction of the moving object, because the network does not distinguish the object movement in one frame. So, whether the object is moving does not affect 3D object representation learning.

Appearance model. Besides the 3D object representation, following the mainstream 2D MOT methods, we use an object re-identification network as the appearance model:

$${}^{(2D)}\mathbf{f}_j^t = \text{ReID}(\mathbf{I}^t, \mathbf{B}_j^t). \quad (7)$$

The architecture of the appearance model is the ResNet50 backbone followed by a global average pooling layer and a fully connected layer with 512 channels. Triplet loss [17] is used for robust appearance feature learning. The appearance model is trained on WOD training set for 20 epochs and the feature is also used for training the object association module, but will not be updated.

Object association. The proposed object association model contains two parts: a GNN-based feature aggregation module and a differentiable matching module. Given the object’s 3D representation and appearance feature, we define the object feature for

$${}^{(0)}\mathbf{f}_j^t = [{}^{(2D)}\mathbf{f}_j^t, {}^{(3D)}\mathbf{f}_j^t], \quad (8)$$

where $[\cdot]$ is the concatenation operation and 3D representation and appearance features are L_2 -normalized first. We adopt an L -layer cross-frame GNN to aggregate the object features from different frames:

$${}^{(l+1)}\mathbf{f}_j^t = \text{MLP}\left({}^{(l)}\mathbf{f}_j^t + \frac{\|{}^{(l)}\mathbf{f}_j^t\|_2 \cdot {}^{(l)}\mathbf{m}_j^{t-1}}{\|{}^{(l)}\mathbf{m}_j^{t-1}\|_2}\right), l \in [0, L-1], \quad (9)$$

where the aggregated message \mathbf{m}_j^{t-1} is calculated from

$${}^{(l)}\mathbf{m}_j^{t-1} = \sum_{j'=1}^{n_{t-1}} ({}^{(l)}w_{j,j'}) \cdot {}^{(l)}\mathbf{f}_{j'}^{t-1}. \quad (10)$$

Averaging weight $w_{j,j'}$ is cosine similarity between the normalized features

$${}^{(l)}w_{j,j'} = \cos({}^{(l)}\mathbf{f}_j^t, {}^{(l)}\mathbf{f}_{j'}^{t-1}). \quad (11)$$

The matching layer is defined as a differentiable Quadratic Problem [16], and the association loss can be the binary cross-entropy loss between the matching results and the matching ground truth.

4.3. Tracking with 3D Object Representation

After obtaining the 3D object representation and training the object association model, we propose our online tracker P3DTrack. In this section, we explain how the tracker infers frame by frame. Similar to DeepSORT [56], we match detections with existing tracklets in each frame. The tracklet’s appearance feature is the average of appearance features in each frame. As for 3D object representation, we utilize a 3D Kalman Filter to model the 3D object motion of the tracklet. The 3D representation of the tracklet is from the predicted 3D position using 3D KF and encoded with Eq. 6. During the object association stage, we use the association model in Sec. 4.2. Besides, we balance the 3D representation and appearance similarity with weight α and $1 - \alpha$, respectively.

5. Experiments

5.1. Dataset and Evaluation Metrics

We conduct our experiments mainly on the large-scale autonomous driving dataset, Waymo Open Dataset (WOD). WOD has 798 sequences for training, 202 for validation, and 150 for testing. More than 1 million images are taken from 5 surrounding cameras. Such a big dataset is suitable for more general feature learning in MOT. The official evaluation metrics are CLEAR MOT metrics [2]. MOTA is the main metric to evaluate the number of false positives, false negatives, and mismatches. The number of mismatches is the most important to evaluate the data association performance. Besides, to evaluate more detailed data association performance, we also report the IDF1 metric [40] using `py-motmetrics`¹ library. The ablation study is conducted with the FRONT camera on WOD val set. To verify the performance of our method in different datasets, we also report the results on KITTI [14] dataset in the appendix.

¹<https://github.com/cheind/py-motmetrics>

Method	Backbone	Split	Category	MOTA \uparrow	IDF1 \uparrow	FN \downarrow	FP \downarrow	ID Sw. \downarrow	MT \uparrow	ML \downarrow
IoU baseline [29]	ResNet-50	val	Vehicle	38.25	-	-	-	-	-	-
Tracktor++ [1, 29]	ResNet-50	val	Vehicle	42.62	-	-	-	-	-	-
RetinaTrack [29]	ResNet-50	val	Vehicle	44.92	-	-	-	-	-	-
QDTrack [12]	ResNet-50	val	Vehicle	55.6	66.2	514548	214998	24309	17595	5559
P3DTrack (Ours)	DLA-34	val	Vehicle	55.9	65.6	638390	74802	37478	13643	8583

Table 1: Results on WOD tracking val set using py-motmetrics library.

5.2. Implementation Details

Training. We use a DLA-34 [58] as the backbone without any neck, and the head is with 2 layers of 3*3 convolutions and MLP. The resolution of the input images is 1920*1280. If the input size is smaller than it, we will use zero padding to complete the image. Our implementation is based on PyTorch [37] framework. We train our model on 8 NVIDIA A40 GPUs. Adam [24] optimizer is applied with $\beta_1 = 0.9$ and $\beta_2 = 0.999$. The learning rate is 8×10^{-5} and weight decay is 10^{-5} . We train 6 epochs for 2D object detection and an additional epoch for 3D object representation learning. The object association module is learned for 4 additional epochs. The cosine learning rate scheduler is adopted. The warm-up stage is the first 500 iterations. In the label generation stage, threshold δ and κ are 0.5 and 30. **Inference.** We set the detection threshold to 0.5 and the bounding box whose score is below the threshold will not create a new tracklet. Similar to ByteTrack [62], the detections with lower scores are matched to the tracklet after the high-quality detections. We set the appearance threshold to 0.6 in data association, and we do not match the pair whose appearance similarity is below the threshold. Like DeepSORT [56], we add an additional 2D IoU-based matching for the remaining detections and tracklets. 3D similarity weight α in matching is set to 0.4. The time interval before we terminate a tracklet, called max-age, is 30 frames.

5.3. Comparisons with State-of-the-art Methods

In Table 1, we show the results compared with SOTA methods on the WOD val set. QDTrack is the previous SOTA method with a FasterRCNN-based detector and the quasi-dense matching learning module. We outperform QDTrack by 0.3 MOTA with a worse DLA-34 backbone. The strict matching strategy and thresholds make the number of FP much lower than QDTrack. The CenterNet-based detector has a lower recall than the FasterRCNN detector in QDTrack, so the FN is much higher than QDTrack and our IDF1 is also suffering from the lower ID Recall problem.

5.4. Ablation Study

We ablate each component in P3DTrack, shown in Table 2. Our baseline is modified DeepSORT [56], but without delayed tracklet initialization. Considering the low-quality detections like ByteTrack [62], the MOTA increases by 2.4.

	MOTA \uparrow	IDF1 \uparrow	FP \downarrow	FN \downarrow	ID Sw. \downarrow
Baseline	51.0	62.3	8709	331056	9100
+low-quality dets [62]	53.4	64.3	13058	309653	9005
+GNN	56.5	66.5	20381	278752	10129
+3D representation	57.6	68.1	33587	258066	9920

Table 2: Ablation study of P3DTrack.

Methods	MOTA \uparrow	IDF1 \uparrow	FP \downarrow	FN \downarrow	ID Sw. \downarrow
2D + 3D feature (Ours)	57.6	68.1	33587	258066	9920
2D feature	56.5	66.5	20381	278752	10129
2D feature + 2D motion	55.5	58.6	29586	263370	23979
2D feature + 3D motion	57.3	63.3	33048	257936	13026

Table 3: Different 2D and 3D representations in P3DTrack.

3D rep from	MOTA \uparrow	IDF1 \uparrow	FP \downarrow	FN \downarrow	ID Sw. \downarrow
P3DTrack (Ours)	57.6	68.1	33587	258066	9920
SfM [44]	55.5	66.8	55823	249935	11145
MiDaS v3 [38]	55.7	63.4	34514	259471	21058

Table 4: Comparisons with different 3D representation.

det thres	app thres	MOTA \uparrow	IDF1 \uparrow	FP \downarrow	FN \downarrow	ID Sw. \downarrow
0.4	0.6	51.4	64.9	117703	210305	17933
0.5	0.6	57.6	68.1	33587	258066	9920
0.6	0.6	50.1	63.0	12885	337208	4864
0.5	0.5	56.1	66.6	41097	257660	13359
0.5	0.7	58.0	66.9	28798	260921	9139

Table 5: Different detection and appearance thresholds.

3D weight α	MOTA \uparrow	IDF1 \uparrow	FP \downarrow	FN \downarrow	ID Sw. \downarrow
0.0 (2D feature)	56.5	66.5	20381	278752	10129
0.4	57.6	68.1	33587	258066	9920
0.5	57.3	67.2	34091	258324	11733
0.6	56.8	66.0	34213	258583	14431
1.0 (3D feature)	52.1	54.2	33366	265203	42443

Table 6: Different 3D representation similarity weight.

Methods	Backbone	Latency	Memory	#Param.
Baseline	DLA-34	219.8ms	13.29GB	22.65M
P3DTrack (Ours)	DLA-34	231.5ms	13.33GB	24.42M

Table 7: Inference latency, training memory, and the number of parameters compared with the baseline model.

With association learning with GNN and jointly learning 3D representation, MOTA and IDF1 metrics can improve by 4.2 and 3.8.



Figure 4: **Qualitative results.** Top: Baseline model without 3D object representation. Bottom: P3DTrack (Ours).

5.5. Discussions

Influence of 3D representation. In P3DTrack, we consider the appearance feature similarity and 3D representation similarity and weight them with α . As shown in Table 3, we conduct experiments to verify this kind of design is better than the method only with appearance features and with 2D Kalman Filter and 3D Kalman Filter motion models. Compared with appearance features only, we have 1.1 MOTA and 1.6 IDF1 improvement. If we use 2D KF to model the motion of bounding boxes, the performance is worse than with appearance features only. That is because the 2D motion cannot be modeled as a linear system, especially for the cars parking on the roadside. The 3D KF is a better motion model. However, without jointly learned 3D representation, the association is still not well enough, especially for the IDF1 metric.

Different 3D representation. We also compare different 3D representation in Table 4. Compared with learning-free Structure-from-Motion 3D positions, our method has the generalization ability to predict the moving objects, but only with SfM the 3D position of the moving object is incorrect. Besides, the pre-trained depth model MiDaS v3 [38] can not estimate video-consistent depth for the object. Based on the relative depth, the 3D motion model can not predict the correct depth in the next frame, which is important to obtain a good 3D similarity.

Influence of detection and appearance thresholds. The detection threshold is to decide the quality of the detections. And the appearance threshold is to avoid the mismatch between the detections and the tracklets. The experiments in Table 5 show these thresholds are necessary for our method. And finally, we choose 0.5 and 0.6 for detection and appearance thresholds to balance the MOTA and IDF1 metrics.

Influence of 3D similarity weight. As mentioned in Sec. 4.3, we weight the 3D similarity and appearance similarity with α . In Table 6, we show the tracking results with different weights. When $\alpha = 0$, we only use the appear-

ance feature to associate the objects. Note that even only with the 3D representation learned from the video, not depending on any image features, the tracking results are not so bad, with 5.1 MOTA and 13.9 IDF1 decreases compared with the best performance. However, with the combination of appearance similarity and 3D representation similarity, the performance is better.

Additional cost compared with baseline. Although we generate the pseudo 3D object labels and train an additional 3D object representation learning module, we do not add much extra computation overhead and memory cost. As shown in Table 7, the inference latency only increases by 12 ms, about 5.5% relatively slower than the baseline. The training memory and the number of network parameters also indicate the efficiency of our method.

5.6. Qualitative Results

We show the qualitative results of baseline and P3DTrack in Fig. 4. When the object is heavily occluded, with 3D representation, P3DTrack can keep the tracklet and avoid mismatching. 3D representation is also useful for similar appearances, the new object will not match the existing tracklet, due to different 3D locations.

6. Conclusion

In this paper, we propose a new 2D MOT framework with the help of 3D object representation from the video itself, called P3DTrack. We design a pseudo 3D object label generation method from the reconstructed scene and 2D bounding boxes with identity. Supervised by the pseudo 3D object labels, the 3D object representation can be jointly learned with 2D object detection and object association. So, an online tracker can be easily achieved with the learnable association module. We conduct experiments mainly on the large-scale Waymo Open Dataset. Extensive experiments show the effectiveness of our method.

Appendix

In the appendix, we describe the detailed network architectures and implementation details, perform additional experiments, and provide more analyses. The contents are as below:

- In Sec. **A** and **B**, we show the details of P3DTrack to help understand our method.
- In Sec. **C**, there are additional experiments on KITTI and analyses about our 3D object learning module.
- In Sec. **D**, visualization shows the success and failure cases.
- In Sec. **E**, we discuss the limitation and future work.
- In Sec. **F**, the reproducibility statement helps reproduce our work.

A. Network Architecture

Module	Keys	Values
DLA-34	levels	1, 1, 1, 2, 2, 1
	channels	16, 32, 64, 128, 256, 512
DLA-up	channels	64, 128, 256, 512
	scales	1, 2, 4, 8
Cls-head-pre	Conv	2* (3*3),64,256
Reg-head-pre	Conv	2* (3*3),64,256
Cls-head	MLP	256,3
Reg-head	MLP	256,4
Offset-head	MLP	256,2
Depth-head	MLP	256,1
Uncer-head	MLP	256,1
App-model	backbone	ResNet50
App-feature	channels	512
3D-feature	channels	512
Obj-feature	fusion	concat&norm
GNN	#layer	1

Table A: Network architecture of P3DTrack

In this section, we explain the detailed network design of P3DTrack. The parameters of the network architecture are shown in Table **A**. The backbone is a standard ‘dla-seg’ architecture, please refer to [67] for more details. The heads include classification head (Cls-head), 2D regression head (Reg-head), offset head (Offset-head), depth and depth uncertainty head (Depth-head & Uncer-head). The appearance model is the ResNet50 backbone followed by a global average pooling layer and a fully connected layer with 512 channels. The 3D object feature is 512 channels predicted by a fully-connected layer from the 3D object position regression. The object feature is fused by concatenating the appearance feature and 3D feature and normalizing it. The object feature is aggregated by 1 layer GNN.

Configuration	Values
optimizer	Adam
optimizer momentum	$\beta_1 = 0.9, \beta_2 = 0.999$
weight decay	1×10^{-5}
learning rate	8×10^{-5}
learning rate scheduler	cosine decay
warmup iterations	500
epochs	6+1+4
augmentation	random flip
aug. probability	0.5
batch size	8
gradient clip	5
image size	1920 × 1280 (zero padding)
loss name	heatmap loss, bbox loss, offset loss depth loss, reid loss, association loss
loss weight	1.0, 1.0, 0.2, 0.1, NA (pretrained), 0.5
sync BN	True

Table B: Training config of P3DTrack.

B. Training Details

In Table **B**, we list the training config of P3DTrack. In P3DTrack, 2D object detection is first learned for 6 epochs and 3D object representation is learned for 1 epochs. Then 3D object representation and object association can be jointly learned for 4 epochs. The appearance model is pre-trained and frozen in the later training stage.

C. Additional Experiments and Analyses

C.1. Results on KITTI Dataset

We conduct some additional experiments on KITTI [14] dataset. KITTI MOT dataset has 21 sequences for training and 29 sequences for testing. The official metrics are mainly based on HOTA [30], including the detection metrics DetA, LocA, and the association metric AssA. KITTI also evaluates the CLEAR MOT [2] metrics. The implementation details of P3DTrack are mostly the same as WOD dataset. However, there are some different settings. We train the 2D detection part for 40 epochs and then train 3D representations for 20 epochs and jointly train the association module for 5 epochs. We use the pre-trained 2D detection model on the general object detection COCO [27] dataset, the same as the other methods evaluated on KITTI. The 3D weight α is set to 0.3, and the detection threshold is 0.2. The basic image resolution is 1280×384. We use additional random resize augmentation. The augmentation probability is 0.5, and the resize scale is random in [0.5,1.5]. We report the tracking results of vehicles.

As shown in Table **C**, we achieve new state-of-the-art performance compared with the methods without any additional human annotations and pre-trained models on the autonomous driving datasets. Especially for the association

Method	+Label	+Data	HOTA	AssA	ID Sw.	DetA	DetRe	DetPr	AssRe	AssPr	LocA	MOTA
QD-3DT [19]	3D GT		72.77	72.19	206	74.09	78.13	85.48	74.87	89.21	87.16	85.94
Mono3DT [18]	3D GT		73.16	74.18	379	72.73	76.51	85.28	77.18	87.77	86.88	84.28
OC-SORT [4]		PD	76.54	76.39	250	77.25	80.64	86.36	80.33	87.17	87.01	90.28
PermaTrack [49]		PD	78.03	78.41	258	78.29	81.71	86.54	81.14	89.49	87.10	91.33
RAM [48]		PD	79.53	80.94	210	78.79	82.54	86.33	84.21	88.77	87.15	91.61
QDTrack [12]			68.45	65.49	313	72.44	76.01	85.37	68.28	88.53	86.50	84.93
TrackMPNN [39]			72.30	70.63	481	74.69	80.02	83.11	73.58	87.14	86.14	87.33
CenterTrack [66]			73.02	71.20	254	75.62	80.10	84.56	73.84	89.00	86.52	88.83
LGM [50]			73.14	72.31	448	74.61	80.53	82.16	76.38	84.74	85.85	87.60
DEFT [5]			74.23	73.79	344	75.33	79.96	83.97	78.30	85.19	86.14	88.38
P3DTrack (Ours)			74.59	76.86	219	72.88	78.09	83.21	80.66	86.67	86.28	85.60

Table C: Tracking results on KITTI *test* set.

	$\delta < 1.25 \uparrow$	$\delta < 1.25^2 \uparrow$	$\delta < 1.25^3 \uparrow$	Abs Rel \downarrow	Sq Rel \downarrow	RMSE \downarrow	RMSE log \downarrow
SfM [44] init.	0.945	0.962	0.967	0.112	1.183	4.744	0.203
P3DTrack (Ours)	0.974	0.983	0.985	0.049	0.456	3.372	0.110
training w/ 3D GT	0.991	0.994	0.995	0.025	0.142	1.999	0.059

Table D: 3D object depth accuracy analyses on KITTI *training* set. We ignore the predictions with depth >75 m.

metrics, we improve AssA by 3.0 and have the lowest number of ID Switches. Because we do not train our model on other autonomous driving datasets, the detection performance is not the best and we do not outperform the methods with a pre-trained model on the PD dataset. However, compared with the monocular 3D MOT methods that use the additional 3D ground truth, we still outperform them.

C.2. 3D Object Location Accuracy Analyses

In Table D and Table E, we discuss the object depth accuracy of our P3DTrack on KITTI and WOD. The metrics are from the general depth estimation metrics [10]. Note that we only calculate the depth accuracy of the object centers. We can find that our P3DTrack, which trains 3D object representation from SfM initialization, has more accurate object depth estimation than the initialized pseudo labels. Note that we only consider the objects that have been assigned 3D pseudo labels when evaluating the SfM initialization. However, for P3DTrack, we evaluate depth of all detected objects, including the generalized objects without initial 3D pseudo labels. Even though, P3DTrack still outperforms the SfM initialization in object 3D location on both KITTI and WOD datasets.

C.3. Gap between Ours and Using 3D GT Labels

Table D and Table E also show the 3D object location accuracy gap between ours and the model trained with ground truth 3D object labels. We find that learning 3D object representation from SfM-initialized pseudo labels is a little

worse than learning from GT 3D labels. However, the gap in 3D location accuracy is relatively small, which means our pseudo labels are practical for estimating the object’s 3D location. The ablation study results in the main paper also show that 3D object representation can help object association. In Table C, the comparison with monocular 3D MOT, QD-3DT and Mono3DT, shows our advantages.

C.4. Dynamic Object 3D Estimation Analyses

As mentioned in Sec. 4.1 and 4.2 of the main paper, we can not assign labels for some objects because they are filtered in pseudo 3D object label generation stage, especially for the dynamic objects that have the different moving directions from the camera. The 3D location of these objects can only be learned by our 3DRL module. In Table F, we validate the performance of generalized 3D location learning for dynamic objects. Most objects are not generated 3D object labels and only 43.6% of the objects (static objects) have pseudo labels. The small gap between dynamic and static objects in results show the generalization of our 3DRL module to the unlabeled dynamic objects.

C.5. Tracking Results of Different Cameras

We report the tracking results conditioned on the camera in Table G. It is obvious that the main FRONT camera has the best performance. The FRONT LEFT and FRONT RIGHT camera has a relatively well performance on both MOTA and IDF1. However, the results of side cameras are not as good as front cameras, because of the rapid move-

	$\delta < 1.25 \uparrow$	$\delta < 1.25^2 \uparrow$	$\delta < 1.25^3 \uparrow$	Abs Rel \downarrow	Sq Rel \downarrow	RMSE \downarrow	RMSE log \downarrow
SfM [44] init.	0.981	0.988	0.990	0.106	0.831	3.973	0.473
P3DTrack (Ours)	0.987	0.992	0.993	0.084	0.653	2.940	0.145
training w/ 3D GT	0.996	0.998	0.998	0.022	0.233	1.569	0.061

Table E: 3D object depth accuracy analyses on WOD *training* set. We ignore the predictions with depth>75m. Note that 3D GT is annotated on LiDAR, so some objects do not have the 3D label. True depth error is lower than the values in table.

	ratio	$\delta < 1.25 \uparrow$	$\delta < 1.25^2 \uparrow$	$\delta < 1.25^3 \uparrow$	Abs Rel \downarrow	Sq Rel \downarrow	RMSE \downarrow	RMSE log \downarrow
Dynamic	56.4%	0.985	0.990	0.992	0.087	0.922	3.349	0.152
Static	43.6%	0.988	0.994	0.995	0.081	0.305	2.305	0.135
All	100%	0.987	0.992	0.993	0.084	0.653	2.940	0.145

Table F: Dynamic/static objects’ 3D location performance on WOD.

	MOTA \uparrow	IDF1 \uparrow	FP \downarrow	FN \downarrow	ID Sw. \downarrow
FRONT	57.6	68.1	33587	258066	9920
FRONT LEFT	58.5	66.6	11782	105092	6874
FRONT RIGHT	55.6	64.1	8566	79516	4765
SIDE LEFT	52.8	61.5	12741	112641	8506
SIDE RIGHT	49.4	59.1	8126	83075	7413

Table G: Tracking results for each camera on WOD *val* set.

ment of the camera relative to the objects and the crowded vehicles in parking lots that are often on the sides. To keep the generalizability and scalability of the algorithm, we do not set specific parameters for the side cameras.

D. Qualitative Results

We provide videos to show the tracking results of P3DTrack on WOD and KITTI datasets. The sequences are ‘segment-7650923902987369309_2380_000_2400_000’ in WOD val set and ‘0011’ in KITTI test set. Please refer to the attachments in the compressed zip file.

E. Limitations and Future Work

In this paper, we estimate the object’s 3D location and represent it as a 3D feature. However, because the monocular depth estimation is an ill-posed problem, the learned object 3D location is not so good, especially for the object far away (>100m). We will try to learn 3D object representation from multi-frames like recent work [15, 25, 52].

F. Reproducibility Statement

We will release the training and inference codes to help reproduce our work and the documents will be clearly written. Pseudo 3D object labeling tools that are based on open-source packages COLMAP [44]² and hloc [42]³ will

²<https://github.com/colmap/colmap>

³<https://github.com/cvg/Hierarchical-Localization>

be released. The checkpoint trained on the KITTI dataset will also be released. Limited by the license of WOD, the checkpoint of the model trained on WOD cannot be publicly available. However, we will provide it by email if needed. The implementation details, including the implementation details, network architecture, and different settings on KITTI are mentioned in Sec. 4 and 5.2 in the main paper and Sec. A, B and C in the appendix. The best hyperparameters of the experiments are listed in Sec. 5.2 in the main paper and Sec. C in appendix, and the influences of hyperparameters are shown in Table 5 and Table 6. The inference latency and computational cost are in Table 7 in the main paper. The data and annotations of WOD⁴ and KITTI⁵ are publicly available.

References

- [1] Philipp Bergmann, Tim Meinhardt, and Laura Leal-Taixe. Tracking without bells and whistles. In *ICCV*, 2019. 7
- [2] Keni Bernardin and Rainer Stiefelagen. Evaluating multiple object tracking performance: the clear mot metrics. *EURASIP Journal on Image and Video Processing*, 2008:1–10, 2008. 6, 9
- [3] Guillem Brasó and Laura Leal-Taixé. Learning a neural solver for multiple object tracking. In *CVPR*, 2020. 1, 2
- [4] Jinkun Cao, Xinshuo Weng, Rawal Khirodkar, Jiangmiao Pang, and Kris Kitani. Observation-centric sort: Rethinking sort for robust multi-object tracking. In *CVPR*, 2023. 10
- [5] Mohamed Chaabane, Peter Zhang, J Ross Beveridge, and Stephen O’Hara. Deft: Detection embeddings for tracking. In *CVPRW*, 2021. 10
- [6] Andrew J Davison. Real-time simultaneous localisation and mapping with a single camera. In *ICCV*, 2003. 3
- [7] Patrick Dendorfer, Vladimir Yugay, Aljosa Osep, and Laura Leal-Taixé. Quo vadis: Is trajectory forecasting the key towards long-term multi-object tracking? In *NeurIPS*, 2022. 1

⁴<https://waymo.com/open/>

⁵https://www.cvlibs.net/datasets/kitti/eval_tracking.php

- [8] Daniel DeTone, Tomasz Malisiewicz, and Andrew Rabinovich. Superpoint: Self-supervised interest point detection and description. In *CVPRW*, 2018. 4
- [9] Mihai Dusmanu, Ignacio Rocco, Tomas Pajdla, Marc Pollefeys, Josef Sivic, Akihiko Torii, and Torsten Sattler. D2-net: A trainable cnn for joint detection and description of local features. *arXiv preprint arXiv:1905.03561*, 2019. 4
- [10] David Eigen, Christian Puhrsch, and Rob Fergus. Depth map prediction from a single image using a multi-scale deep network. In *NeurIPS*, 2014. 10
- [11] Lue Fan, Feng Wang, Naiyan Wang, and Zhaoxiang Zhang. Fully sparse 3d object detection. In *NeurIPS*, 2022. 3
- [12] Tobias Fischer, Jiangmiao Pang, Thomas E Huang, Linlu Qiu, Haofeng Chen, Trevor Darrell, and Fisher Yu. Qdtrack: Quasi-dense similarity learning for appearance-only multiple object tracking. *arXiv preprint arXiv:2210.06984*, 2022. 7, 10
- [13] Martin A Fischler and Robert C Bolles. Random sample consensus: a paradigm for model fitting with applications to image analysis and automated cartography. *Communications of the ACM*, 24(6):381–395, 1981. 4
- [14] Andreas Geiger, Philip Lenz, and Raquel Urtasun. Are we ready for autonomous driving? the kitti vision benchmark suite. In *CVPR*, 2012. 6, 9
- [15] Jiawei He, Yuntao Chen, Naiyan Wang, and Zhaoxiang Zhang. 3d video object detection with learnable object-centric global optimization. In *CVPR*, 2023. 3, 11
- [16] Jiawei He, Zehao Huang, Naiyan Wang, and Zhaoxiang Zhang. Learnable graph matching: Incorporating graph partitioning with deep feature learning for multiple object tracking. In *CVPR*, 2021. 1, 2, 6
- [17] Alexander Hermans, Lucas Beyer, and Bastian Leibe. In defense of the triplet loss for person re-identification. *arXiv preprint arXiv:1703.07737*, 2017. 6
- [18] Hou-Ning Hu, Qi-Zhi Cai, Dequan Wang, Ji Lin, Min Sun, Philipp Krahenbuhl, Trevor Darrell, and Fisher Yu. Joint monocular 3d vehicle detection and tracking. In *ICCV*, 2019. 2, 10
- [19] Hou-Ning Hu, Yung-Hsu Yang, Tobias Fischer, Trevor Darrell, Fisher Yu, and Min Sun. Monocular quasi-dense 3d object tracking. *IEEE Transactions on Pattern Analysis and Machine Intelligence*, 45(2):1992–2008, 2022. 10
- [20] Junjie Huang, Guan Huang, Zheng Zhu, and Dalong Du. Bevdet: High-performance multi-camera 3d object detection in bird-eye-view. *arXiv preprint arXiv:2112.11790*, 2021. 2
- [21] Rudolph Emil Kalman. A new approach to linear filtering and prediction problems. 1960. 2
- [22] Alex Kendall and Yarin Gal. What uncertainties do we need in bayesian deep learning for computer vision? In *NeurIPS*, 2017. 6
- [23] Tarasha Khurana, Achal Dave, and Deva Ramanan. Detecting invisible people. In *ICCV*, 2021. 1
- [24] Diederik P Kingma and Jimmy Ba. Adam: A method for stochastic optimization. *arXiv preprint arXiv:1412.6980*, 2014. 7
- [25] Yin hao Li, Han Bao, Zheng Ge, Jinrong Yang, Jianjian Sun, and Zeming Li. Bevstereo: Enhancing depth estimation in multi-view 3d object detection with dynamic temporal stereo. *arXiv preprint arXiv:2209.10248*, 2022. 3, 11
- [26] Zhiqi Li, Wenhai Wang, Hongyang Li, Enze Xie, Chonghao Sima, Tong Lu, Yu Qiao, and Jifeng Dai. Bevformer: Learning bird’s-eye-view representation from multi-camera images via spatiotemporal transformers. In *ECCV*, 2022. 2
- [27] Tsung-Yi Lin, Michael Maire, Serge Belongie, James Hays, Pietro Perona, Deva Ramanan, Piotr Dollár, and C Lawrence Zitnick. Microsoft coco: Common objects in context. In *ECCV*, 2014. 9
- [28] David G Lowe. Distinctive image features from scale-invariant keypoints. *International journal of computer vision*, 60(2):91–110, 2004. 3
- [29] Zhichao Lu, Vivek Rathod, Ronny Votel, and Jonathan Huang. Retinatrack: Online single stage joint detection and tracking. In *CVPR*, 2020. 7
- [30] Jonathon Luiten, Aljosa Osep, Patrick Dendorfer, Philip Torr, Andreas Geiger, Laura Leal-Taixé, and Bastian Leibe. Hota: A higher order metric for evaluating multi-object tracking. *International journal of computer vision*, 129:548–578, 2021. 9
- [31] Xuan Luo, Jia-Bin Huang, Richard Szeliski, Kevin Matzen, and Johannes Kopf. Consistent video depth estimation. *ACM Transactions on Graphics (ToG)*, 39(4):71–1, 2020. 3
- [32] Tim Meinhardt, Alexander Kirillov, Laura Leal-Taixe, and Christoph Feichtenhofer. Trackformer: Multi-object tracking with transformers. In *CVPR*, 2022. 1, 2
- [33] Raul Mur-Artal, Jose Maria Martinez Montiel, and Juan D Tardos. Orb-slam: a versatile and accurate monocular slam system. *IEEE transactions on robotics*, 31(5):1147–1163, 2015. 3
- [34] Richard A Newcombe, Steven J Lovegrove, and Andrew J Davison. Dtam: Dense tracking and mapping in real-time. In *ICCV*, 2011. 3
- [35] Ziqi Pang, Jie Li, Pavel Tokmakov, Dian Chen, Sergey Zagoruyko, and Yu-Xiong Wang. Standing between past and future: Spatio-temporal modeling for multi-camera 3d multi-object tracking. In *CVPR*, 2023. 3
- [36] Dennis Park, Rares Ambrus, Vitor Guizilini, Jie Li, and Adrien Gaidon. Is pseudo-lidar needed for monocular 3d object detection? In *ICCV*, 2021. 2, 3
- [37] Adam Paszke, Sam Gross, Francisco Massa, Adam Lerer, James Bradbury, Gregory Chanan, Trevor Killeen, Zeming Lin, Natalia Gimeshein, Luca Antiga, et al. Pytorch: An imperative style, high-performance deep learning library. In *NeurIPS*, 2019. 7
- [38] René Ranftl, Katrin Lasinger, David Hafner, Konrad Schindler, and Vladlen Koltun. Towards robust monocular depth estimation: Mixing datasets for zero-shot cross-dataset transfer. *IEEE Transactions on Pattern Analysis and Machine Intelligence*, 44(3), 2022. 7, 8
- [39] Akshay Rangesh, Pranav Maheshwari, Mez Gebre, Siddhesh Mhatre, Vahid Ramezani, and Mohan M Trivedi. Trackmpnn: A message passing graph neural architecture for multi-object tracking. *arXiv preprint arXiv:2101.04206*, 2021. 10

- [40] Ergys Ristani, Francesco Solera, Roger Zou, Rita Cucchiara, and Carlo Tomasi. Performance measures and a data set for multi-target, multi-camera tracking. In *ECCV*, 2016. 6
- [41] Fatemeh Saleh, Sadeh Aliakbarian, Hamid Rezaatfighi, Mathieu Salzmann, and Stephen Gould. Probabilistic tracklet scoring and inpainting for multiple object tracking. In *CVPR*, 2021. 2
- [42] Paul-Edouard Sarlin, Cesar Cadena, Roland Siegwart, and Marcin Dymczyk. From coarse to fine: Robust hierarchical localization at large scale. In *CVPR*, 2019. 11
- [43] Paul-Edouard Sarlin, Daniel DeTone, Tomasz Malisiewicz, and Andrew Rabinovich. Superglue: Learning feature matching with graph neural networks. In *CVPR*, 2020. 4
- [44] Johannes Lutz Schönberger and Jan-Michael Frahm. Structure-from-motion revisited. In *CVPR*, 2016. 2, 3, 4, 7, 10, 11
- [45] Johannes Lutz Schönberger, Enliang Zheng, Marc Pollefeys, and Jan-Michael Frahm. Pixelwise view selection for unstructured multi-view stereo. In *ECCV*, 2016. 3
- [46] Shaoshuai Shi, Chaoxu Guo, Li Jiang, Zhe Wang, Jianping Shi, Xiaogang Wang, and Hongsheng Li. Pv-rnn: Point-voxel feature set abstraction for 3d object detection. In *CVPR*, 2020. 3
- [47] Zhi Tian, Chunhua Shen, Hao Chen, and Tong He. Fcos: Fully convolutional one-stage object detection. In *ICCV*, 2019. 4
- [48] Pavel Tokmakov, Allan Jabri, Jie Li, and Adrien Gaidon. Object permanence emerges in a random walk along memory. In *ICML*, 2022. 10
- [49] Pavel Tokmakov, Jie Li, Wolfram Burgard, and Adrien Gaidon. Learning to track with object permanence. In *ICCV*, 2021. 10
- [50] Gaoang Wang, Renshu Gu, Zuozhu Liu, Weijie Hu, Mingli Song, and Jenq-Neng Hwang. Track without appearance: Learn box and tracklet embedding with local and global motion patterns for vehicle tracking. In *ICCV*, 2021. 10
- [51] Qitai Wang, Yuntao Chen, Ziqi Pang, Naiyan Wang, and Zhaoxiang Zhang. Immortal tracker: Tracklet never dies. *arXiv preprint arXiv:2111.13672*, 2021. 1, 2
- [52] Tai Wang, Jiangmiao Pang, and Dahua Lin. Monocular 3d object detection with depth from motion. In *ECCV*, 2022. 3, 11
- [53] Tai Wang, Xinge Zhu, Jiangmiao Pang, and Dahua Lin. Fcos3d: Fully convolutional one-stage monocular 3d object detection. In *ICCV*, 2021. 2
- [54] Yue Wang, Vitor Campagnolo Guizilini, Tianyuan Zhang, Yilun Wang, Hang Zhao, and Justin Solomon. Detr3d: 3d object detection from multi-view images via 3d-to-2d queries. In *CoRL*, 2022. 2
- [55] Xinshuo Weng, Jianren Wang, David Held, and Kris Kitani. Ab3dmot: A baseline for 3d multi-object tracking and new evaluation metrics. *arXiv preprint arXiv:2008.08063*, 2020. 2
- [56] Nicolai Wojke, Alex Bewley, and Dietrich Paulus. Simple online and realtime tracking with a deep association metric. In *ICIP*, 2017. 1, 2, 6, 7
- [57] Yihong Xu, Aljosa Osep, Yutong Ban, Radu Horaud, Laura Leal-Taixé, and Xavier Alameda-Pineda. How to train your deep multi-object tracker. In *CVPR*, 2020. 2
- [58] Fisher Yu, Dequan Wang, Evan Shelhamer, and Trevor Darrell. Deep layer aggregation. In *CVPR*, 2018. 4, 7
- [59] Fangao Zeng, Bin Dong, Yuang Zhang, Tiancai Wang, Xiangyu Zhang, and Yichen Wei. Motr: End-to-end multiple-object tracking with transformer. In *ECCV*, 2022. 1, 2
- [60] Tianyuan Zhang, Xuanyao Chen, Yue Wang, Yilun Wang, and Hang Zhao. Mutr3d: A multi-camera tracking framework via 3d-to-2d queries. In *CVPR*, 2022. 2
- [61] Yunpeng Zhang, Jiwen Lu, and Jie Zhou. Objects are different: Flexible monocular 3d object detection. In *CVPR*, 2021. 2, 3, 6
- [62] Yifu Zhang, Peize Sun, Yi Jiang, Dongdong Yu, Fucheng Weng, Zehuan Yuan, Ping Luo, Wenyu Liu, and Xinggang Wang. Bytetrack: Multi-object tracking by associating every detection box. In *ECCV*, 2022. 2, 7
- [63] Yifu Zhang, Chunyu Wang, Xinggang Wang, Wenjun Zeng, and Wenyu Liu. Fairmot: On the fairness of detection and re-identification in multiple object tracking. *International Journal of Computer Vision*, 129(11):3069–3087, 2021. 5
- [64] Zhoutong Zhang, Forrester Cole, Richard Tucker, William T Freeman, and Tali Dekel. Consistent depth of moving objects in video. *ACM Transactions on Graphics (TOG)*, 40(4):1–12, 2021. 3
- [65] Tinghui Zhou, Matthew Brown, Noah Snavely, and David G Lowe. Unsupervised learning of depth and ego-motion from video. In *CVPR*, 2017. 3
- [66] Xingyi Zhou, Vladlen Koltun, and Philipp Krähenbühl. Tracking objects as points. In *ECCV*, 2020. 10
- [67] Xingyi Zhou, Dequan Wang, and Philipp Krähenbühl. Objects as points. *arXiv preprint arXiv:1904.07850*, 2019. 4, 9
- [68] Xingyi Zhou, Tianwei Yin, Vladlen Koltun, and Philipp Krähenbühl. Global tracking transformers. In *CVPR*, 2022. 1, 2